Mechanism of Synergism between Antimicrobial Peptides Magainin 2 and PGLa[†]

Katsumi Matsuzaki,*[,‡] Yasuyuki Mitani,[‡] Ken-ya Akada,[‡] Osamu Murase,[‡] Shuji Yoneyama,[‡] Michael Zasloff,[§] and Koichiro Miyajima[‡]

Graduate School of Pharmaceutical Sciences, Kyoto University, Sakyo-ku, Kyoto 606-8501, Japan, and Magainin Research Institute, 5110 Campus Drive, Plymouth Meeting, Pennsylvania 19462

Received May 18, 1998; Revised Manuscript Received July 13, 1998

ABSTRACT: The antimicrobial peptides magainin 2 and PGLa, discovered in the skin of the African clawed frog, *Xenopus laevis*, exhibit marked synergism [Westerhoff, H. V., Zasloff, M., Rosner, J. L., Hendler, R. W., de Waal, A., Vaz Gomes, A., Jongsma, A. P. M., Riethorst, A., and Juretic, D., *Eur. J. Biochem. 228*, 257−264 (1995)], although the mechanism is not yet clear. They are believed to kill bacteria by permeabilizing membranes. In this study, we examined the interactions of these peptides in lipid bilayers. PGLa, like magainin 2, preferentially interacts with acidic lipids, forming an amphipathic helix. The peptide induces the release of a water-soluble dye, calcein, entrapped within liposomes. The coexistence of magainin 2 enhances membrane permeabilization, which is maximal at a 1:1 molar ratio. Fluorescence experiments using L18W-PGLa revealed that both peptides form a stoichiometric 1:1 complex in the membrane phase with an association free energy of −15 kJ/mol. Single amino acid mutations in magainin 2 significantly altered the synergistic activity, suggesting that precise molecular recognition is involved in complex formation. The complex as well as each component peptide form peptide−lipid supramolecular complex pores, which mediate the mutually coupled transbilayer transport of dye, lipid, and the peptide per se. The rate of pore formation rate is in the order complex ≥ PGLa > magainin 2, whereas the pore lifetime is in the order magainin 2 > complex > PGLa. Therefore, the synergism is a consequence of the formation of a potent heterosupramolecular complex, which is characterized by fast pore formation and moderate pore stability.

The granular glands, specialized neuroepithelial cells in amphibian skin, store and secrete a number of biologically active peptides (*1*). Magainin 2 (*2*) and PGLa (*3*) (Figure 1) were discovered in this structure of the African clawed frog, *Xenopus laevis*, and exhibit a broad spectrum of antimicrobial activity as well as tumoricidal properties (*4*). These cationic peptides electrostatically recognize anionic lipids on the surface of microbes and transformed cells to permeabilize the cell membranes, leading to cell death (*4*−*6*). The lack of significant toxicity against normal mammalian cells makes these peptides promising candidates as novel antibiotics for medical use (*4*, *7*). Interestingly, although the individual peptides are highly potent, mixtures of magainin 2 and PGLa show marked functional synergism in bacteria, tumor cells, and artificial lipid membranes (*1*, *8*−*10*). This phenomenon is of biological and clinical importance, but little is known about the mechanism except that the peptides appear to form a putative, highly potent 1:1 stoichiometric complex.

A large number of studies have been carried out to elucidate the mechanism of magainin-induced membrane permeabilization. For a review, see ref 11. We proposed the following model. The peptide forms an amphipathic helix in lipid bilayers, which essentially lies parallel to the membrane surface (*12*, *13*). Five helices on average, together with several surrounding lipids, form a membrane-spanning pore comprising a dynamic, peptide−lipid supramolecular complex, which allows not only ion transport but also a rapid flip-flop of the membrane lipids (*14*). Upon disintegration of the pore, a fraction of the peptide molecules stochastically translocates into the inner leaflet (*15*, *16*). These processes can be controlled by modifying the peptide charge (*17*).

In contrast, there have been few reports on PGLa−membrane interactions. The peptide also preferentially

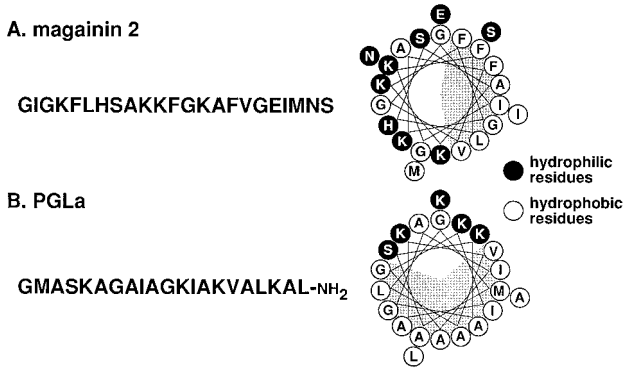

FIGURE 1: The amino acid sequences and the helical wheel representations of (A) magainin 2 and (B) PGLa. The shaded area indicates the hydrophobic surface of the amphipathic helix.

[†] Supported by the Research Foundation for Pharmaceutical Sciences and a Grant-in-Aid for Encouragement of Young Scientists (09771946) from the Ministry of Education, Science, and Culture of Japan.

* To whom correspondence should be addressed. Telephone: 81-75-753-4574. Fax: 81-75-761-2698. E-mail: katsumim@pharm.kyoto-u.ac.jp.

[‡] Kyoto University.

[§] Magainin Research Institute.

10.1021/bi9811617 CCC: $15.00
Published on Web 10/09/1998

interacts with acidic phospholipids, forming an α-helix (*18*, *19*), which lies parallel to the membrane surface (*20*). The presence of negatively charged phospholipids enhances the membrane permeabilizing activity (*9*), which may be related to PGLa-induced formation of acidic lipid-rich domains (*19*).

In this study, we systematically investigated the interactions of PGLa and magainin 2−PGLa mixtures with phospholipid bilayers, and the results were compared with those of magainin 2. The three systems were found to have essentially the same mode of interaction, i.e., formation of a peptide−lipid supramolecular complex pore. The magainin pore was characterized by a relatively long lifetime, although the formation rate was relatively slow. In contrast, PGLa frequently forms unstable pores. Magainin 2 and PGLa form a 1:1 complex in the membrane phase, which retains both advantages, namely, fast pore formation and moderate pore stability.

MATERIALS AND METHODS

Materials. Magainin peptides and L18W-PGLa were synthesized by a standard Fmoc-based solid-phase method, as previously described (*13*). The purity of the synthesized peptides was determined by analytical HPLC[1] and ion spray mass spectroscopy. PGLa was provided by Magainin Pharmaceuticals, Inc. (Plymouth Meeting, PA). EYPG was a kind gift from Asahi Kasei Co. (Tokyo, Japan). DNS-PE and C_6-NBD-PC were purchased from Avanti Polar Lipids (Alabaster, AL). The other phospholipids and FITC−dextran were obtained from Sigma (St. Louis, MO). Calcein and spectrograde organic solvents were supplied by Dojindo (Kumamoto, Japan). All other chemicals from Wako (Tokyo, Japan) were of special grade. A Tris−HCl buffer (10 mM Tris/150 mM NaCl/1 mM EDTA, pH 7.0) was prepared from double-distilled water.

Vesicle Preparation. LUVs were prepared and characterized as described elsewhere (*14*). Briefly, a lipid film, after drying under vacuum overnight, was hydrated with a 70 mM calcein solution (pH adjusted to 7.0 with NaOH) or the buffer and vortex-mixed to produce MLVs. The suspension was freeze−thawed for five cycles and then successively extruded through polycarbonate filters (a 0.6 μm pore size filter, 5 times; two stacked 0.1 μm pore size filters, 10 times). SUVs for CD measurements were produced by sonication of the freeze−thawed MLVs in ice/water under a nitrogen atmosphere. The lipid concentration was determined in triplicate by phosphorus analysis (*21*).

Calcein Leakage. Vesicles containing calcein were separated from free calcein on a Bio-gel A-1.5m column. If necessary, calcein-free LUVs were mixed with dye-loaded liposomes to adjust the lipid concentration to the desired value. The release of calcein from the LUVs was fluorometrically monitored on a Shimadzu RF-5000 spectrofluorometer at an excitation wavelength of 490 nm and an emission wavelength of 520 nm at 30 °C. The maximum fluorescence intensity corresponding to 100% leakage was determined by the addition of 10% w/v Triton X-100 (20 μL) to 2 mL of the sample. The apparent percent leakage value was calculated according to eq 1. F and F_t denote

$$\% \text{ apparent leakage} = 100(F - F_0)/(F_t - F_0) \quad (1)$$

the fluorescence intensity before and after addition of the detergent, respectively. F_0 represents the fluorescence of intact vesicles. Experimental errors were usually within 5%.

FITC−Dextran Leakage. A double-labeling method was utilized (*22*). LUVs of EYPC/EYPG/DNS-PE (50/48.5/1.5) entrapping 3 mM FITC−dextran (MW 4400) were incubated with the peptide for 5 min. A 5 mg/mL trypsin solution (500 μL) was added to stop membrane permeabilization. The leaked FITC−dextran was removed by gel filtration (Biogel, A-1.5m). The excitation spectrum of the vesicle fraction after solubilization with Triton X-100 was measured at an emission wavelength of 520 nm. The method used to calculate the percent leakage value has been reported elsewhere (*22*).

Peptide Association. The association of the peptides in the membrane was determined on the basis of tryptophan fluorescence. Peptide solutions were incubated with LUVs for 10 min at 30 °C. Fluorescence spectra in the range of 300−400 nm were measured on a Hitachi F-4500 spectrofluorometer at an excitation wavelength of 280 nm. The spectra were corrected for both wavelength-dependent effects (*23*) and intensity loss due to light scattering after subtraction of the corresponding blank spectra with corresponding nonfluorescent peptides. The latter correction was carried out by use of indoxyl sulfate (*13*).

CD Spectra. CD spectra were measured on a Jasco J-720 apparatus interfaced to an NEC PC-9801 microcomputer, using a 1-mm path length quartz cell to minimize the absorbance due to buffer components. The instrumental outputs were calibrated with nonhygroscopic ammonium *d*-camphor-10-sulfonate (*24*). Eight scans were averaged for each sample, and the averaged blank spectra (the vesicle suspension) were subtracted. The peptide concentration was 25 μM. The absence of any optical artifacts was confirmed as described elsewhere (*25*).

RET. Dansyl-labeled LUVs were prepared by hydrating the lipid film composed of EYPC, EYPG, and DNS-PE in a molar ratio of 50:45:5. RET from the Trp residue of the peptide to the dansyl chromophore in the membrane was monitored by observing the fluorescence intensity of either the Trp residue (336 nm) or the dansyl group (510 nm) upon excitation at 280 nm. The temperature was controlled at 30 ± 0.5 °C.

Flip-Flop. The peptide-induced lipid flip-flop was detected as previously reported (*14*). NBD-labeled LUVs were generated from an equimolar mixture of EYPC and EYPG containing 0.5 mol % C_6-NBD-PC. The symmetrically labeled vesicles were mixed with 1 M sodium dithionite/1 M Tris ([lipid] = 8 mM, [dithionite] = 60 mM) and

[1] Abbreviations: BBPS, bovine brain L-α-phosphatidyl-L-serine; CD, circular dichroism; C_6-NBD-PC, 1-palmitoyl-2-[6-((7-nitrobenz-2-oxa-1,3-diazol-4-yl)amino)caproyl]-L-α-phosphatidylcholine; DNS-PE, *N*-[[(5-(dimethylamino)naphthyl]-1-sulfonyl] egg yolk L-α-phosphatidylethanolamine; DPoPE, dipalmitoleoyl-L-α-phosphatidylethanolamine; EYPC, egg yolk L-α-phosphatidylcholine; EYPG, L-α-phosphatidyl-DL-glycerol enzymatically converted from EYPC.; Fmoc, fluoren-9-ylmethoxycarbonyl; FITC−dextran, fluorescein isothiocyanate−dextran of MW 4400; HPLC, high-performance liquid chromatography; LUVs, large unilamellar vesicles; MIC, minimum inhibitory concentration; MLVs, multilamellar vesicles; L/P, lipid-to-peptide molar ratio; PC, phosphatidylcholine; PG, phosphatidylglycerol; P/L, peptide-to-lipid molar ratio; RET, resonance energy transfer; SUVs, small unilamellar vesicles; T_H, lamellar-to-hexagonal II phase transition temperature.

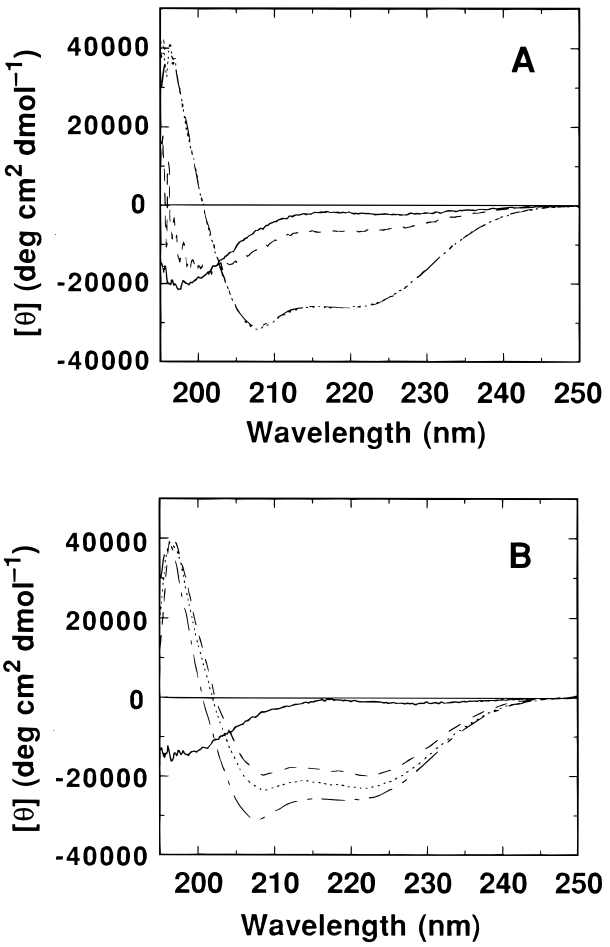

FIGURE 2: CD spectra. The CD spectra of PGLa, magainin 2, and their 1:1 mixture were measured at 30 °C ([peptide] = 25 μM). (A) The spectra of PGLa in a Tris buffer (10 mM Tris/150 mM NaCl/1 mM EDTA, pH 7.0), 0.6 mM EYPG SUVs, 0.6 mM BBPS SUVs, and 1.4 mM EYPC SUVs are denoted by solid, dotted, dashed, and broken curves, respectively. (B) The spectra of the mixed peptides in the buffer and 0.6 mM PG are shown by the solid and dotted curves. The broken and dashed traces represent the spectra of magainin 2 and PGLa, respectively, in the presence of 0.6 mM EYPG SUVs.

incubated for 15 min at 30 °C to produce inner leaflet-labeled vesicles. The vesicles were immediately separated from dithionite by gel filtration (Bio-gel A-1.5m, 1.5 cm × 18 cm column). The fraction of NBD-lipids which had flopped during incubation in the absence or presence of the peptide was measured on the basis of fluorescence quenching by sodium dithionite. The asymmetrically NBD-labeled LUVs (2.0 mL) were incubated with or without the peptide for various periods at 30 °C. In the case of the peptide-containing samples, 500 μL of a trypsin solution (5 mg/mL) was added to 1.5 mL samples and reacted for 5 min to hydrolyze the peptide. After 40 μL of a 1 M sodium dithionite/1 M Tris solution had been added, NBD fluorescence was monitored on a Shimadzu RF-5000 spectrofluorometer in which the cuvette holder was thermostatically maintained at 30 ± 0.5 °C. The excitation and emission wavelengths were 450 and 530 nm, respectively. The percent flip-flop value was calculated according to (*14*).

Antibacterial Activity. The MIC values of magainin 2, PGLa, and their 1:1 mixture against *Escherichia coli* (ATCC 8739) were determined as previously described (*13*). Briefly, bacterial cells (10^6 cfu/mL) in the midlogarithmic growth phase were incubated with various concentrations of sterilized peptides (1.6, 3.1, 6.3, 13, 25, 50, and 100 μM) in the presence of nutrients for 4 h at 37°C. Bacterial growth was determined from the optical density at 405 nm.

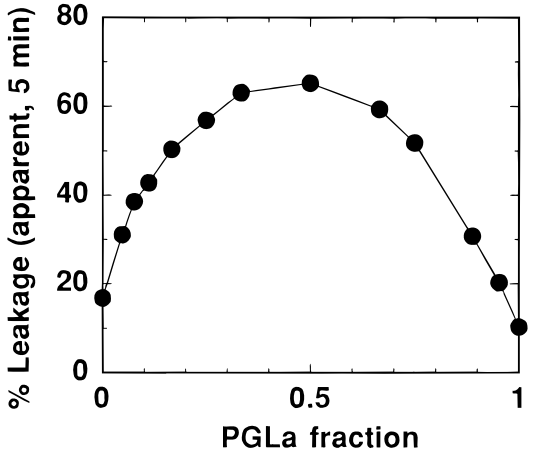

FIGURE 3: Synergism in membrane permeabilization. Mixtures of magainin 2 and PGLa were incubated with calcein-loaded EYPG LUVs for 5 min at a peptide concentration of 1.5 μM ([lipid] = 490 μM). The apparent percent leakage value is plotted as a function of PGLa fraction. The temperature was controlled at 30 ± 0.5 °C.

RESULTS

CD. Figure 2A shows that PGLa adopted an unordered structure in the buffer (solid curve). In contrast, the peptide bound to acidic BBPS (dashed trace) and EYPG bilayers (dotted trace), forming an α-helix (P/L = 24). The perfectly superimposable spectra were characterized by double minima at 208 and 222 nm. Further addition of vesicles caused no changes in the spectra. The helical wheel representation of PGLa (Figure 1) indicated that the peptide can form an amphipathic helix with a wider hydrophobic angle than magainin 2. The existence of zwitterionic EYPC vesicles induced only a minor spectral change even at a higher P/L of 55 (broken curve). The presence of an isodichroic point at 203 nm indicated a two-state equilibrium: the membrane-bound conformation of PGLa was the same in both anionic and zwitterionic membranes. The affinity of the peptide for the latter bilayers was, however, much smaller. Figure 2B depicts the spectra of a 1:1 magainin 2−PGLa mixture. In the buffer, the mixed peptide exhibited no defined secondary structure (solid curve), suggesting that the peptides do not form a complex in aqueous solution. In EYPG bilayers (dotted curve), the spectrum was close but not identical to the numerical average of those of magainin 2 (broken trace) and PGLa (dashed trace), indicating that there were no marked conformational changes, even if both peptides formed a complex in the lipidic environment.

Synergism in Membrane Permeabilization. Membrane permeabilizing activity was examined by a dye release assay. Mixtures of magainin 2 and PGLa were incubated with calcein-loaded EYPG vesicles at a constant P/L value of 1/306. Figure 3 shows the apparent percent leakage value at 5 min plotted as a function of PGLa molar fraction. Maximum permeabilization was observed at a PGLa fraction of 0.5, suggesting that a 1:1 stoichiometric complex is involved in synergism. Synergism was also detected in other model membrane systems and bacteria (Table 1, see also Figure 7A).

Table 1: Synergism in Various Systems

system	magainin 2	PGLa	1:1 mixture
		$(P/L)_{50}$[a]	
BBPS LUVs	0.051	0.026	0.011
EYPC LUVs	0.57	0.14	0.05
		MIC (μM)	
E. coli	50	50	6.3

[a] Peptide-to-lipid molar ratio at which 50% apparent dye release was observed during 5 min incubation at 30 °C. The estimation error was typically within 10%.

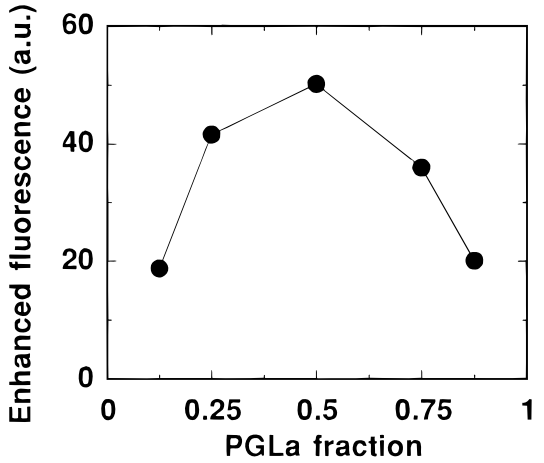

FIGURE 4: Stoichiometry of magainin 2−PGLa complex. The fluorescence spectra of L18W-PGLa in the presence of 102 μM EYPG/EYPC (1/1) LUVs were recorded at peptide concentrations of 0.5, 1, 2, 3, and 3.5 μM. Magainin 2 was then added at concentrations of 3.5, 3, 2, 1, and 0.5, respectively, to keep the total peptide concentration constant (4 μM). Enhancement in fluorescence intensity by the coexistence of magainin 2 is plotted as a function of PGLa fraction.

Heterosupramolecular Complex Formation. Formation of a magainin−PGLa heterosupramolecular complex was fluorometrically detected. For this purpose, a fluorescent PGLa analogue, L18W-PGLa, was synthesized. Confirmation of the equipotency of the mutant peptide is important. The dye releasing activity of L18W-PGLa was almost identical to that of the underivatized peptide in the absence or presence of equimolar magainin 2 (data not shown). Clearly, Trp substitution did not modify the properties of PGLa.

The stoichiometry of the complex was determined by the continuous variation method (*26*) on the basis of the observation that complex formation enhanced the quantum yield of Trp fluorescence. First, the fluorescence spectra of L18W-PGLa in the presence of 102 μM EYPG/EYPC (1/1) LUVs were recorded at peptide concentrations of 0.5, 1, 2, 3, and 3.5 μM. Magainin 2 was then added at concentrations of 3.5, 3, 2, 1, and 0.5, respectively, to keep the total peptide concentration constant (4 μM). Under these conditions, the peptides were almost completely membrane-bound. The fluorescence spectra of the mixed peptide systems had larger intensities because of complex formation. The intensity enhancement is proportional to the amount of the complex. Figure 4 shows that the intensity increase was the largest at a PGLa fraction of 0.5, further corroborating the formation of a 1:1 complex.

To estimate the L18W-PGLa−magainin 2 association constant, the Trp fluorescence spectra of L18W-PGLa in EYPG LUVs were measured in the presence of various concentrations of magainin 2. We used pure EYPG to ensure complete peptide binding even at higher P/L values. Complex formation resulted in a slight blue shift (1−2 nm) and a quantum yield enhancement (spectra not shown). The intensity at 336 nm increased from 99.0 to 136.4 upon complex formation. The latter value was evaluated by extrapolation of the intensity versus 1/[magainin 2] plot to 1/[magainin 2] $\rightarrow$ 0. Using these extremes, we calculated the extent of complexation, y, at each magainin 2 concentration.

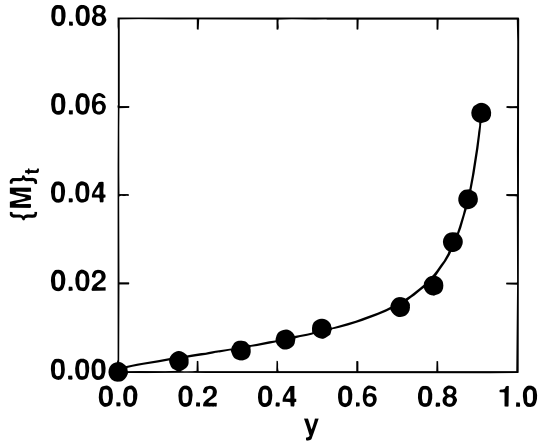

FIGURE 5: Estimation of L18W-PGLa−magainin 2 complex formation constant. The total magainin concentration, $\{M\}_t$, expressed as P/L is plotted against y, the extent of complex formation. The solid trace is one of the best fit curves with $n = 1$ and $K_C = 470$ in eq 5.

$$y = n\{C\}/(\{P\} + n\{C\}) \quad (2)$$

L18W-PGLa, magainin 2, and the 1:1 complex are denoted by P, M, and C, respectively. The brace represents the intramembrane concentration as expressed by the number of moles of each peptide species per mole of lipid. Accurate determination of the association constant, K_C, of equilibrium I required the self-association constant of magainin 2, K_M,

$$n\mathrm{P} + n\mathrm{M} \rightleftharpoons \mathrm{C} \quad (\mathrm{I})$$

because the peptide formed an oligomer in the concentration range used (*13*).

$$m\mathrm{M} \rightleftharpoons \mathrm{M_m} \quad (\mathrm{II})$$

$$K_M = \{M_m\}/\{M\}^m \quad (3)$$

$$K_C = \{C\}/\{P\}^n\{M\}^n \quad (4)$$

The values of K_M and m were estimated to be 33 and 2, respectively (see Appendix). The total magainin concentration, $\{M\}_t$, can be described as follows:

$$\{M\}_t = \{M\} + m\{M_m\} + n\{C\}$$

$$= (1/\{P\}_t(1-y))(y\{P\}_t/nK_C)^{1/n} + mK_M(1/\{P\}_t(1-y))^m(y\{P\}_t/nK_C)^{m/n} + y\{P\}_t \quad (5)$$

The total L18W-PGLa concentration was denoted by $\{P\}_t$. Figure 5 plots $\{M\}_t$ versus y. Any integer n can well explain the data. For $n = 1$, 2, 3, and 4, the best K_C values were

4.7×10^2, 1.3×10^7, 4.6×10^{11}, and 1.9×10^{16}, respectively. The solid curve is one of the best-fit curves with $n = 1$ and $K_C = 470$. If we did not take the self-association of magainin 2 into consideration, the fitting was much poorer.

Mutant Experiments. The above results strongly suggested that magainin 2 and PGLa form a 1:1 stoichiometric complex. If this was the case, a single amino acid substitution at the recognition site would significantly influence the synergism. We therefore examined the synergism between PGLa and several magainin analogues based on calcein release from EYPG/EYPC (1/1) LUVs. PGLa alone, one of the magainin mutants alone, or their 1:1 mixture was incubated with the calcein-loaded LUVs for 5 min at various peptide concentrations while the lipid concentration was kept constant (ca. 400 μM). The apparent percent dye leakage value was plotted as a function of P/L, and $(P/L)_{50}$, a P/L value at which 50% leakage was observed, was determined. To quantitatively compare synergism, a synergistic factor, *S*, was defined by eq 6.

$$S = (P/L)_{50\text{calcd}}/(P/L)_{50\text{obsd}} \quad (6)$$

The observed $(P/L)_{50}$ of the 1:1 mixture is denoted by $(P/L)_{50\text{obsd}}$. $(P/L)_{50\text{calcd}}$ represents the $(P/L)_{50}$ value in the case of no synergism calculated from the dose−response curves of the individual peptides. The *S* values were 3.3, 3.6, 1.7, and 1.6 for magainin 2, F5W-magainin 2, F16W-magainin 2, and E19Q-magainin 2 amide, respectively. Furthermore, an unrelated 14-residue peptide, mastoparan X, exhibited no synergism with magainin 2 or PGLa ($S = 1$), although this peptide also forms a peptide−lipid supramolecular complex pore in bilayers (*27*). Thus, synergism appeared to involve the formation of a magainin−PGLa supramolecule with precise molecular recognition.

Pore Lifetime. The efficient dye release caused by the peptide mixture can be attributed to a high pore forming rate and/or a long pore lifetime, because as described below the mechanism of membrane permeabilization is essentially the same for F5W-magainin 2, PGLa, and the mixture.[2] The lifetime of the pore, τ, can be evaluated by determination of the extent of self-quenching of the peptide-treated, calcein-entrapped LUVs (*28*). After mixing the calcein-containing EYPG/EYPC (1/1) LUVs (415 μM) with various amounts of the peptide at 30 °C, the time course of calcein fluorescence increase was monitored in a cuvette for 5 min. Aliquots (500 μL) of the liposome suspension were immediately sampled into Eppendorf tubes containing 500 μL of a trypsin solution (5 mg/mL) to immediately and completely stop leakage. Triton X-100 was added to the cuvette to lyse the vesicles. The apparent retention, *E*, was calculated according to eq 7.

$$E = (F_t - F)/(F_t - F_0) \quad (7)$$

The apparent percent leakage (eq 1) is equal to $100(1 - E)$. In addition, the liposomes in the Eppendorf tube were applied to a Bio-gel A-1.5m column. The vesicle fraction was separated from the leaked calcein by gel filtration, and its quenching factor (*Q*) was obtained by measuring the fluorescence intensity before (F_b) and after (F_a) the addition of Triton X-100.

$$Q = F_b/F_a \quad (8)$$

The *Q* value was plotted against the *E* value in Figure 6.

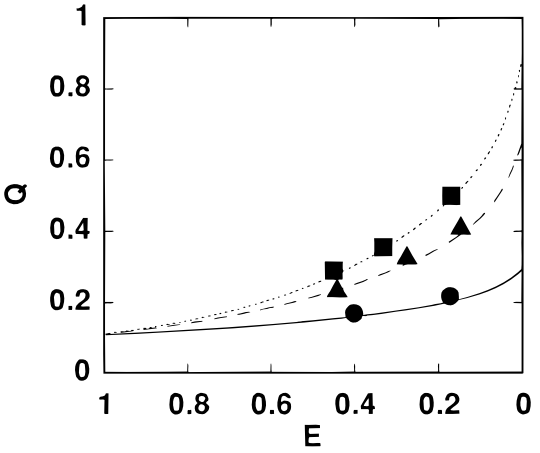

FIGURE 6: Estimation of the pore lifetime at 30 °C. The apparent retention, *E* (eq 7), is shown against the quenching factor, *Q* (eq 8). Peptide: ●, F5W-magainin 2; ■, PGLa; ▲, 1:1 mixture. Theoretical curves for $\rho = 0.2$ (solid), 0.6 (broken), and 0.9 (dotted) calculated according to Schwarz (*28*) are shown. See the text for details.

Schwarz introduced a dimensionless parameter, ρ, to describe the pore life span (*28*).

$$\rho = \tau_0/(\tau + \tau_0) \quad (9)$$

τ_0 is the time necessary for a 1/*e* reduction of the intravesicular dye concentration. Theoretical *Q* vs *E* curves for various ρ values were calculated as reported (*28*). Comparison of the theoretical values with the data obtained (Figure 6) indicated the ρ values for F5W-magainin 2 (circles), PGLa (squares), and the mixture (triangles) to be 0.2, 0.9, and 0.6, respectively, corresponding to $\tau = 4\tau_0$, $0.1\tau_0$, and $0.7\tau_0$. The estimation error in ρ was ± 0.05.

The τ_0 value may differ among the three cases, because it is inversely proportional to the pore cross-sectional area. To estimate the pore size, we examined the leakage of a larger solute, FITC−dextran (MW 4400) (*22*). Its dimensions as an oblate are approximately 2 nm × 4 nm, whereas those of calcein are 1 nm × 2 nm. Figure 7A clearly shows that none of the peptides induced leakage of the larger solute at P/L values where ca. 80% calcein release was observed, indicating that the diameters of each pore were comparable (ca. 2 nm). Therefore, the τ_0 value can be assumed to be identical for the three systems (ca. 3 ms). However, it should be noted that the pore size was dependent on P/L. The mixture induced leakage of FITC−dextran at a much higher P/L value of 0.01 (Figure 7A).

We now know that the pore lifetime is in the order F5W-magainin 2 > mixture > PGLa. The number of calcein-permeable pores formed per vesicle, *p*, during 5 min was calculated as a measure of pore formation rate according to eq 10 and is plotted as a function of P/L in Figure 7B.

$$p = -(\ln R)/(1 - \rho) \quad (10)$$

[2] In the following experiments, we used F5W-magainin 2 instead of magainin 2 to monitor peptide translocation. The fluorescent peptide mimics the parent peptide in its intrinsic membrane permeabilization activity (*13*) as well as synergism with PGLa (vide supra).

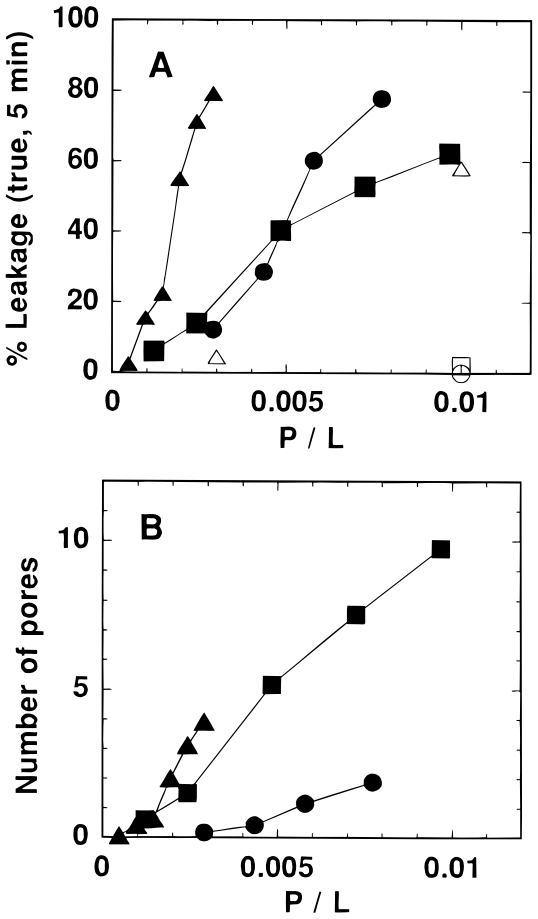

FIGURE 7: Membrane permeabilization and pore formation. (A) The true percent leakage of calcein (MW 623, closed symbols) and FITC−dextran (MW 4400, open symbols) from EYPG/EYPC (1/1) LUVs during 5 min incubation at 30 °C are plotted as a function of P/L. Peptides: ●, F5W-magainin 2; ■, PGLa; ▲, 1:1 mixture. (B) The number of pores formed during 5 min incubation was calculated from the dose−response curves for calcein release in (A) and the pore lifetime (Figure 6), according to eq 10 (*28*).

The true retention of the dye, *R*, was obtained from the apparent retention, *E*, by the method of Schwarz (*28*). Figure 7B demonstrated that the pore formation rate of magainin was much smaller than that of PGLa, although once formed the magainin pore is much more stable. The mixed peptide was found to be an effective pore former, comparable to or even better than PGLa. In conclusion, the synergism is a consequence of fast pore formation and moderate pore stability.

Peptide Translocation. Translocation of the peptide across lipid bilayers was detected as reported elsewhere (*15*). The technique measures the amount of the untranslocated peptides remaining in the outer monolayers. The untranslocated peptides can be readily removed from the vesicle surface by extraction with a large excess of a second population of vesicles. The unremovable fraction was determined by RET from the Trp residue of the peptide to the dansyl chromophore (DNS-PE) incorporated into the membrane phase.

Figure 8 shows that the addition of dansyl-labeled LUVs (EYPC/EYPG/DNS-PE = 50/45/5) to an L18W-PGLa solution at time zero (P/L = 1/414) resulted in a significant decrease in Trp fluorescence, indicating RET due to the binding of the peptide to the membrane. After a short

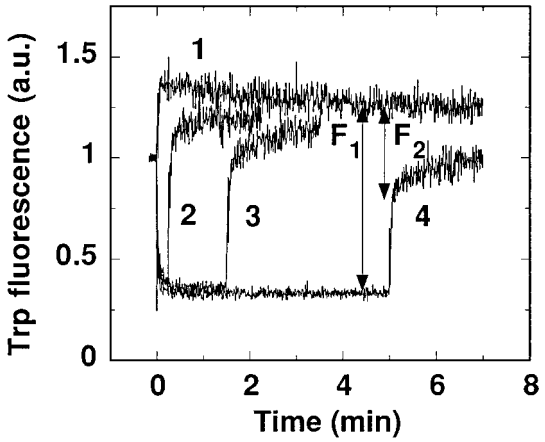

FIGURE 8: Detection of the peptide translocation (1). L18W-PGLa was mixed with dansyl-LUVs (EYPC/EYPG/DNS-PE = 5/4.5/0.5) at time zero. The final peptide and lipid concentrations were 1 and 414 μM, respectively. The fluorescence intensity of Trp at 336 nm (excited at 280 nm) was recorded. Binding of the peptide to the vesicles reduced the intensity because of RET. After various incubation periods (0.25, 1.5, and 5 min, traces 2−4), a large excess (final concentration ca. 2 mM) of the second population of dansyl-free EYPG SUVs was added. An increase in intensity indicates the relief from RET caused by the redistribution between the two vesicle populations of the peptide molecules which had been bound to the outer surface of the first vesicle. The increased intensity decreased with prolonged incubation and was smaller than the fluorescence intensity when both populations of vesicles were simultaneously added at time zero (trace 1), thus indicating that some of the peptides were translocated into the inner leaflet during the incubation.

incubation for 15 s, a second population of EYPG SUVs[3] (2 mM) was added in large excess (trace 2). An increase in the fluorescence intensity implied that the peptide molecules, which had been bound to the *outer* leaflet, were redistributed between the two vesicle populations, resulting in relief from RET. The increased fluorescence intensity was, however, smaller than the intensity when both populations of vesicles were added simultaneously to the peptide solution at time zero (trace 1), suggesting that a fraction of the peptides became unexposed to the outer surface and were therefore untransferable to the second vesicles. The buried fraction increased with incubation time (traces 2−5), indicating time-dependent translocation of the peptide. The percent translocation was calculated as follows (*15*):[4]

$$\% \text{ translocation} = 100 \times F_2/F_1 \qquad (11)$$

The time courses of translocation and dye leakage for F5W-magainin 2, L18W-PGLa, and the 1:1 mixture are plotted in Figure 9. In all cases, the peptide internalization (closed symbols) was completely coupled with true dye release (solid traces).[5]

We then examined translocation of the individual peptides in the peptide mixture by use of Trp-labeled and native peptides (Table 2). Comparison of the data for the homo-

[3] EYPG was used instead of EYPG/EYPC due to the much faster extraction of the untranslocated peptide. The use of SUVs reduces light scattering, which interferes with precise determination of the extent of translocation.

[4] The peptide might translocate via aqueous pores if a significant fraction was present as the free form. However, this possibility was excluded because we carried out the experiments under conditions where the peptide was almost completely bound.

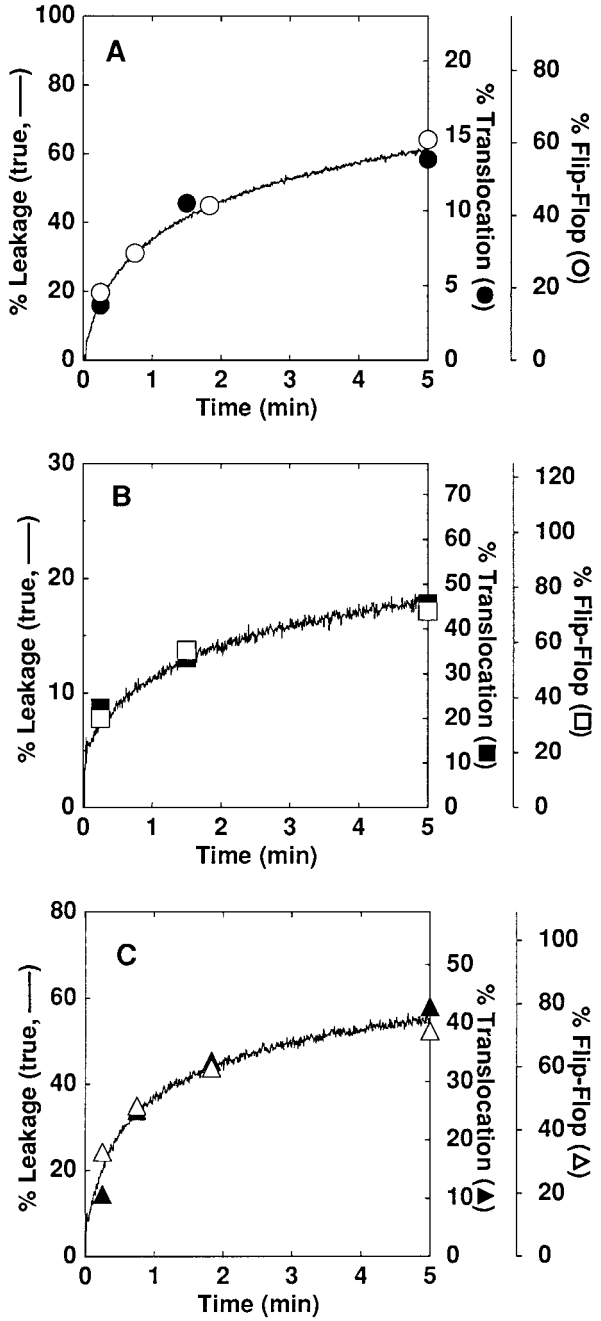

FIGURE 9: Coupling between dye leakage, peptide translocation, and lipid flip-flop. Time courses of calcein true leakage (solid curves), translocation (closed symbols), and flip-flop (open symbols) are shown for (A) F5W-magainin 2, (B) L18W-PGLa, and (C) 1:1 mixture. The peptide concentrations were 2.4, 1.0, and 0.8 μM, respectively; [lipid] = 414 μM.

mixtures (F5W-magainin 2/magainin 2 versus L18W-PGLa/PGLa) revealed that the translocation efficiency of PGLa was greater than that of magainin 2 by virtue of the high pore forming tendency (Figure 7A) and short pore lifetime (Figure 6) of the former. The coexistence of PGLa greatly facilitated the internalization of F5W-magainin 2. In the heteromixture (magainin 2/L18W-PGLa), L18W-PGLa also effectively passed through the bilayer. The PGLa/magainin 2 translocation ratio in the 1:1 mixture was greater than unity (48/36) because free PGLa molecules which do not participate in heterosupramolecular complex formation can also be efficiently internalized.

The enhanced translocation of F5W-magainin 2 in the presence of PGLa was further confirmed by another method (*15*). Trypsin was encapsulated within the internal aqueous phase of EYPC/EYPG/DNS-PE (50/45/5) LUVs to selectively digest the translocated peptide. The enzyme hydrolyzes the peptide bonds on the C-terminal sides of the Lys residues. The hydrolyzed Trp-containing fragment, WLHSA, will be desorbed from the membrane and can be detected by the RET technique; desorption resulted in relief from RET, i.e., a decrease in dansyl fluorescence at 510 nm when excited at 280 nm, where Trp was selectively excited. Trace 2 in Figure 10 shows that F5W-magainin 2 in the presence of equimolar magainin 2 was gradually digested by the enzyme within the vesicles, directly indicating that the peptide actually reached the inner leaflet. The enzyme outside the vesicles was inactivated by addition of the

Table 2: Translocation of the Individual Peptides in Peptide Mixtures

mixture (1:1, mol)	% translocation of Trp-containing peptide[a]
F5W-magainin 2/magainin 2	11
F5W-magainin 2/PGLa	36
magainin 2/L18W-PGLa	48
L18W-PGLa/PGLa	45

[a] The mixed peptides (2 μM) were incubated with EYPC/EYPG/DNS-PE (50/45/5) LUVs (414 μM) for 5 min. The percent translocation of the Trp-substituted peptide was determined. The estimation error was 5%.

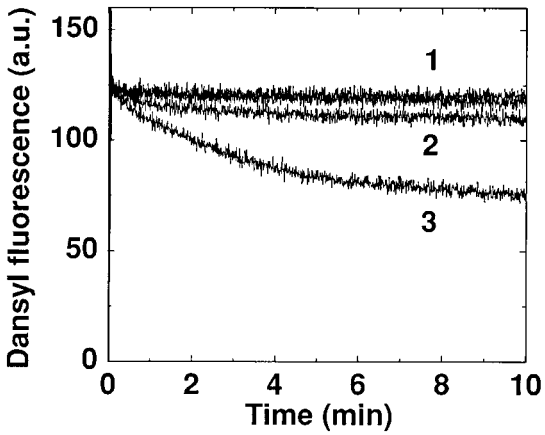

FIGURE 10: Detection of peptide translocation (2). A lipid film (EYPC/EYPG/DNS-PE = 50/45/5) was hydrated with a 200 μM trypsin solution and LUVs were prepared. Trypsin−chymotrypsin inhibitor (400 μM) was externally added to inactivate the enzyme outside the vesicles. F5W-magainin 2 (1.5 μM) was added to the membranes in the presence of either 1.5 μM magainin 2 (traces 1 and 2) or 1.5 μM PGLa (trace 3). The sensitized dansyl fluorescence at 510 nm was recorded upon excitation of Trp residues at 280 nm. Fluorescence decrease implied digestion of the fluorescent peptide by the enzyme within the liposomes, i.e., internalization of the peptide. The enzyme inhibitor was also present inside the LUVs in trace 1. No digestion was observed. The lipid concentration was 216 μM.

[5] The numbers of translocated peptide molecules per vesicle during 5 min were ca. 80, 40, and 50 for Figure 9A, B, and C, respectively, whereas the corresponding *p* values were 0.6, 1.6, and 1.3. Assuming that a pore involves 5 peptide molecules on the average (*16*), the number of peptide molecules participating in pore formation was at most 8, which is much smaller than the above values. We previously encountered a similar problem (*17*). Our tentative explanation is that the peptides also form somewhat smaller, calcein-impermeable pores.

trypsin−chymotrypsin inhibitor (MW ca. 8000). The replacement of magainin 2 by PGLa significantly enhanced internalization of the fluorescent magainin peptide (trace 3). While the membrane is permeable to FITC−dextran (MW 4400) under this condition (Figure 7A), trace 3 suggests that the inhibitor does not easily enter the internal aqueous phase of the liposome. Trace 1 depicts a control experiment where the inhibitor was present on both sides of the vesicle. No digestion was detectable.

Lipid Flip-Flop. The open symbols in Figure 9 represent the time course of lipid flip-flop for F5W-magainin 2, L18W-PGLa, and their 1:1 mixture. In all cases, the transbilayer movement of the fluorescent lipid was completely coupled with both pore formation (solid curves) and peptide translocation (closed symbols).

DISCUSSION

PGLa. The lipid specificity of cationic PGLa is very similar to that of magainin 2. It preferentially binds to acidic phospholipids such as PG and PS, forming an amphipathic helix at physiological ionic strength (Figure 2A), as well as at much lower salt concentrations (*18, 19*), suggesting the importance of electrostatic interactions. This anionic lipid preference of the peptide can well explain its selective toxicity (*5, 19, 29*).

Figure 9B clearly shows that the mechanism of PGLa-induced permeabilization of EYPG/EYPC bilayers is essentially the same as that of magainin 2, i.e., the formation of a peptide−lipid supramolecular complex pore. Magainin 2 imposes positive curvature strain on the membrane, facilitating the formation of torus-type pores (*30*). This conclusion was drawn from the observations that (1) the peptide raises the T_H of DPoPE and (2) the incorporation of reversed-phase inducing lipids, such as PS or PE, markedly inhibited pore formation. PGLa as well as a magainin 2−PGLa 1:1 mixture also raised the T_H of DPoPE (Epand, R. M., personal communication). Furthermore, pore formation in PS membranes was significantly suppressed compared with PG-based bilayers (cf. Figure 7A and Table 1).

PGLa, which has a smaller polar angle than magainin 2 (Figure 1), forms pores more effectively (Figure 7B). Wieprecht et al. synthesized a series of magainin 2 analogues with different angles subtended by the positively charged helix face (*31*). A decrease in angle enhanced pore formation, in keeping with our results. The much shorter lifetime of the PGLa pore (Figure 6) can be ascribed to a positive charge (+5) larger than that of magainin 2 (+3 to +4), because the pores are destabilized by electrostatic repulsions between side chains (*17*).

Synergism. Many studies have been performed with the aim of applying antimicrobial peptides to clinical use, such as the examination of structure−activity relationships (*7, 32−34*) and efficient large-scale peptide production (*35−37*). Enhancement of efficacy by the combined use of antibiotic agents is also an attractive strategy. β-Lactam antibiotics were reported to potentiate the antibacterial activity of magainin 2 both in vitro and in vivo (*38*). This phenomenon may be understood on the basis of antibiotics-induced changes in bacterial outer membrane structure, which facilitate entry of the peptide into the inner membrane.

The mechanism of synergism between magainin 2 and PGLa is completely different. They form a 1:1 supramolecular complex in the membrane phase (Figures 3 and 5) with precise molecular recognition. For $n = 1$, 2, 3, and 4 in eq 5, the Gibbs free energy of complex formation, $\Delta G_C = -RT \ln K_C$, is −15, −41, −68, and −94 kJ/mol.[6] ΔG_C can be expressed by eq 12. ΔG_{MP} is the free energy

$$\Delta G_C = n\Delta G_{MP} + (n-1)\Delta G_{CC} \qquad (12)$$

necessary for the formation of 1 mole of magainin−PGLa complex and ΔG_{CC} is the free energy of complex−complex interaction. These possible ΔG_C values can be well explained by assuming $\Delta G_{MP} = -15$ kJ/mol and $\Delta G_{CC} = -12$ kJ/mol. It is presently not clear if the 1:1 complex further self-aggregates, i.e., $n \geq 2$.

The magainin−PGLa complex also induces membrane permeabilization coupled with peptide translocation and lipid flip-flop (Figure 9C). Therefore, the mechanism of action is essentially the same as that of each component peptide. The high potency of the supramolecule is characterized by fast pore formation (Figure 7B) and a moderate pore lifetime (Figure 6). The former feature can be at least partly ascribable to the difference in the preaggregate formation free energy. ΔG_{MP} (−15 kJ/mol) is larger in magnitude than the free energy of magainin dimer formation, $\Delta G_M = -RT \ln K_M = -8.8$ kJ/mol. We could not evaluate the energy of PGLa oligomerization because the fluorescence spectrum of L18W-PGLa was independent of the intramembrane peptide concentration (data not shown). This latter observation further corroborated the idea that the charge density is a major determining factor of pore stability.

In the above discussion, we did not consider binding of the peptide to the membrane, because we carried out the experiments under conditions where the peptides were almost completely membrane-bound. The direct partitioning of the magainin 2−PGLa complex to the bilayer can be excluded because the complex was not formed in the aqueous phase (Figure 2B). Therefore, each peptide separately binds to the membrane, forming the supramolecule in the bilayer. The complex formation reaction (equilibrium I) shifts the partitioning equilibrium of each component peptide toward enhanced binding, although the partition coefficient itself remains unchanged. Thus, the synergism is partially due to increased binding.

In summary, magainin 2 and PGLa, antimicrobial peptides discovered from the same origin, exhibited marked synergism in permeabilization of lipid bilayers composed of various lipid species. The synergism is ascribable to the formation of a potent, 1:1 stoichiometric complex in the membrane phase with an association free energy of −15 kJ/mol. The supramolecule retains the advantages of both component peptides, i.e. moderate pore stability from magainin 2 and high pore formation rate from PGLa. The complex structure should be elucidated in future studies.

[6] The ΔG value depends on the concentration unit used in the definition of K_C. The use of mole fraction is usually recommended, although this is still a matter of debate (*39*). Our P/L unit was almost equivalent to mole fraction because the intramembrane peptide concentration was rather small.

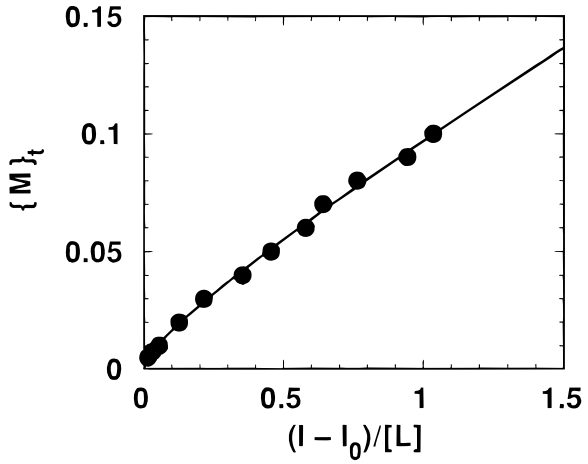

FIGURE 11: Determination of aggregation parameters. $\{M\}_t$ is plotted as a function of $(I - I_0)/[L]$. I is the fluorescence intensity of F16W-magainin 2 at 336 nm. I_0 is that of the bound monomer estimated by linear extrapolation of the I versus $\{M\}_t$ plot to $\{M\}_t \rightarrow 0$. The lipid concentration in μM is denoted by [L]. The trace was drawn by use of eq A1 with $m = 2$, $K_M = 33$, and $\alpha = 15$.

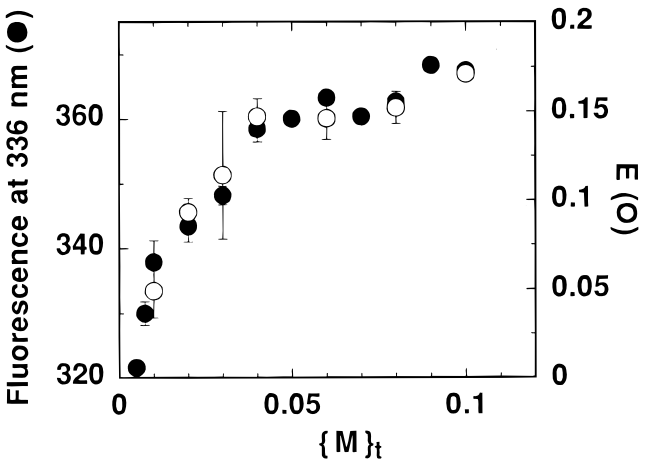

FIGURE 12: RET. The efficiency of RET from Tyr to Trp, E, was determined for an F5Y-magainin 2/F16W-magainin 2 (4 μM/2 μM) mixture in EYPG LUVs at 30 °C. E (○) and I (●) are plotted as a function of $\{M\}_t$. The fluorescence increase is ascribable to peptide self-association.

APPENDIX

We previously reported that the binding isotherms of F5W-, F12W-, and F16W-magainin 2 to EYPG LUVs are sigmoidal, suggesting intramembrane peptide oligomerization (*13*). The self-association constant, K_M, of magainin 2 was estimated as follows by use of F16W-magainin 2, which is equipotent to magainin 2 (*13*). The fluorescence spectra of the peptide (6 μM) were recorded in the presence of EYPG LUVs. From the binding isotherm, we know that the peptide is almost completely membrane-bound (>95%) at L/P values above 10 at this peptide concentration. Addition of lipid caused an intensity decrease and a red shift with an isoemissive point around 353 nm, suggesting that the peptide is in a bound monomer−bound oligomer equilibrium (spectra not shown). The K_M value was evaluated as follows:

$$\{M\}_t = \{M\} + m\{M_m\}$$

$$= [(1/mK_M\alpha)(I - I_0)/[L]]^{1/m} + (1/\alpha)(I - I_0)/[L] \quad \text{(A1)}$$

I denotes the fluorescence intensity at 336 nm. I_0 is the I value in the bound monomeric state, which was estimated by extrapolation of the I versus $\{M\}_t$ plot to $\{M\}_t \rightarrow 0$. The lipid concentration is expressed by [L]. α is the difference in I between the bound oligomer and the bound monomer. Figure 11 plots $\{M\}_t$ against $(I - I_0)/[L]$. The best fits were obtained when $m = 2.0 \pm 0.1$, $K_M = 40 \pm 20$, and $\alpha \approx 15$. The parameter m was then fixed as 2. K_M and α values of 33 ± 9 and 15 ± 1 most satisfactorily explained the results.

To confirm that the spectral change truly reflects peptide aggregation, we carried out RET experiments. F5Y-magainin 2 and F16W-magainin 2 were used as donor and acceptor, respectively. The donor and acceptor were mixed in a molar ratio of 2:1,[7] and the fluorescence spectra were recorded in the emission wavelength range 300−400 nm at an excitation wavelength of 280 nm. The spectra, $F_{YW}(\lambda)$, were curve-fitted in the range 310−340 nm by a linear combination of two spectra in the absence of RET.

$$F_{YW}(\lambda) = aF_Y(\lambda) + bF_W(\lambda) \quad \text{(A2)}$$

$F_Y(\lambda)$ and $F_W(\lambda)$ are the spectra of F5Y-magainin 2/magainin 2 (2/1) and magainin 2/F16W-magainin 2 (2/1), respectively. The presence of RET is characterized by $a < 1$ (quenched donor fluorescence) and $b > 1$ (sensitized acceptor fluorescence). The RET efficiency, E, was calculated by $E = 1 - a$. In aqueous solution, no RET was detected ($a = b = 1$), whereas in the presence of EYPG LUVs, $\{M\}_t$-dependent RET was observed (Figure 12, open circles).[8] The change in E perfectly paralleled the fluorescence enhancement of F16W-magainin 2 (Figure 12, solid circles), strongly indicating that the fluorescence increase was due to the self-aggregation of magainin 2.

The implicit assumption of this experiment was that the fluorescent analogues behave very similarly to the parent magainin 2. We confirmed the validity of this assumption by measuring calcein release from EYPG LUVs at P/L = 1/167. The percent apparent leakage values during 5 min were 50.5 ± 1.6, 49.7 ± 0.4, and 52.5 ± 0.1 for F5Y-magainin 2/F16W-magainin 2 (2/1), F5Y-magainin 2/magainin 2 (2/1), and magainin 2/F16W-magainin 2 (2/1), respectively. Schümann et al. failed to detect peptide aggregation using RET between the F16W-magainin 2 amide and N^{α}-dansyl magainin 2 amide (*41*). The dansylation and/or amidation may change the aggregational behavior of the peptide.

Using $m = 2$ and $K_M = 33$, we calculated the extent of aggregation at each $\{M\}_t$ in Figure 12. E was proportional to the extent of aggregation (not shown), and the E value of the aggregate was estimated to be 0.24 from its slope.

[7] In RET experiments, a donor:acceptor ratio of 1:1 is commonly used. However, we used 2:1 because the Tyr fluorescence is much weaker than the Trp fluorescence.

[8] There could be spontaneous RET even in the absence of any aggregation. According to the two-dimensional RET theory (*40*), the efficiency of this transfer depends on both {acceptor} and the donor−acceptor closest approach. In our case, the magainin helix occupied an area of ca. 3 nm × 1 nm in the bilayer, which may be approximated by a circle with a radius of 1 nm. Therefore, the closest approach was about 2 nm, which is larger than the critical transfer distance of the Tyr-Trp pair (1.4 nm). In this case, the spontaneous RET was negligible.

It should be noted that the possible maximum E value was 0.33 because the donor/acceptor (2/1) mixture was used. Therefore, the intrinsic E value of the dimer was 0.24/0.33 = 0.73. The 5Y−16W distance, R, was evaluated as 1.2 ± 0.1 nm from eq A3 (*42*). The critical transfer distance, R_0,

$$R = R_0[(1 - E)/E]^{1/6} \qquad \text{(A3)}$$

was calculated as 1.4 nm according to Förster (*42*), assuming that the mutual time-averaged orientation of the donor and the acceptor is random. This commonly used assumption is especially reasonable in the case of Trp because indole is characterized by two linear transition moments (*43*).

REFERENCES

1. Bevins, C. L., and Zasloff, M. (1990) *Annu. Rev. Biochem. 59*, 395−414.
2. Zasloff, M. (1987) *Proc. Natl. Acad. Sci. U.S.A. 84*, 5449−5453.
3. Hoffmann, W., Richter, K., and Kreil, G. (1983) *EMBO J. 2*, 711−714.
4. Jacob, L., and Zasloff, M. (1994) in *Antimicrobial Peptides* (Boman, H. G., Marsh, J., and Goode, J. A., Eds.) pp 197−223, John Wiley and Sons, Chichester.
5. Matsuzaki, K., Sugishita, K., Fujii, N., and Miyajima, K. (1995) *Biochemistry 34*, 3423−3429.
6. Matsuzaki, K., Sugishita, K., Harada, M., Fujii, N., and Miyajima, M. (1997) *Biochim. Biophys. Acta 1327*, 119−130.
7. Maloy, W. L., and Kari, U. P. (1995) *Biopolymers 37*, 105−122.
8. Williams, R. W., Starman, R., Taylor, K. M. P., Gable, K., Beeler, T., and Zasloff, M. (1990) *Biochemistry 29*, 4490−4496.
9. Vaz Gomes, A., de Waal, A., Berden, J. A., and Westerhoff, H. V. (1993) *Biochemistry 32*, 5365−5372.
10. Westerhoff, H. V., Zasloff, M., Rosner, J. L., Hendler, R. W., de Waal, A., Vaz Gomes, A., Jongsma, A. P. M., Riethorst, A., and Juretic, D. (1995) *Eur. J. Biochem. 228*, 257−264.
11. Matsuzaki, K. (1998) *Biochim. Biophys. Acta* in press.
12. Bechinger, B., Zasloff, M., and Opella, S. J. (1993) *Protein Sci. 2*, 2077−2084.
13. Matsuzaki, K., Murase, O., Tokuda, H., Funakoshi, S., Fujii, N., and Miyajima, K. (1994) *Biochemistry 33*, 3342−3349.
14. Matsuzaki, K., Murase, O., Fujii, N., and Miyajima, K. (1996) *Biochemistry 35*, 11361−11368.
15. Matsuzaki, K., Murase, O., Fujii, N., and Miyajima, K. (1995) *Biochemistry 34*, 6521−6526.
16. Matsuzaki, K., Murase, O., and Miyajima, K. (1995) *Biochemistry 34*, 12553−12559.
17. Matsuzaki, K., Nakamura, A., Murase, O., Sugishita, K., Fujii, N., and Miyajima, K. (1997) *Biochemistry 36*, 2104−2111.
18. Jackson, M., Mantsch, H. H., and Spencer, J. (1992) *Biochemistry 31*, 7289−7293.
19. Latal, A., Degovics, G., Epand, R. F., Epand, R. M., and Lohner, K. (1997) *Eur. J. Biochem. 248*, 938−946.
20. Bechinger, B., Zasloff, M., and Opella, S. J. (1998) *Biophys. J. 74*, 981−987.
21. Bartlett, G. R. (1959) *J. Biol. Chem. 234*, 466−468.
22. Matsuzaki, K., Yoneyama, S., and Miyajima, K. (1997) *Biophys. J. 73*, 831−838.
23. Melhuish, W. H. (1962) *J. Opt. Soc. Am. 52*, 1256−1258.
24. Takakuwa, T., Konno, T., and Meguro, H. (1985) *Anal. Sci. 1*, 215−218.
25. Matsuzaki, K., Nakai, S., Handa, T., Takaishi, Y., Fujita, T., and Miyajima, K. (1989) *Biochemistry 28*, 9392−9398.
26. Cantor, C. R., and Schimmel, P. R. (1980) in *Biophysical Chemistry*, pp 1135−1138, W. H. Freeman and Co., New York.
27. Matsuzaki, K., Yoneyama, S., Murase, O., and Miyajima, K. (1996) *Biochemistry 35*, 8450−8456.
28. Schwarz, G., and Arbuzova, A. (1995) *Biochim. Biophys. Acta 1239*, 51−57.
29. Lohner, K., and Epand, R. M. (1997) *Adv. Biophys. Chem. 6*, 53−66.
30. Matsuzaki, K., Sugishita, K., Ishibe, N., Ueha, M., Nakata, S., Miyajima, K., and Epand, R. M. (1998) *Biochemistry 37*, 11856−11863.
31. Wieprecht, T., Dathe, M., Epand, R. M., Beyermann, M., Krause, E., Maloy, W. L., MacDonald, D. L., and Bienert, M. (1997) *Biochemistry 36*, 12869−12880.
32. Cuervo, J. H., Rodrigues, B., and Houghten, R. A. (1988) *Pept. Res. 1*, 81−86.
33. Bessalle, R., Haas, H., Goria, A., Dhalit, I., and Fridkin, M. (1992) *Antimicrob. Agents Chemother. 36*, 313−317.
34. Chen, H.-C., Brown, J. H., Morell, J. L., and Huang, C. M. (1988) *FEBS Lett. 236*, 462−466.
35. Sharma, A., Khoury-Christianson, A. M., White, S. P., Dhanjal, N. K., Huang, W., Paulhiac, C., Friedman, E. J., Manjula, B. N., and Kumar, R. (1994) *Proc. Natl. Acad. Sci. U.S.A. 91*, 9337−9341.
36. Faber, K. N., Westra, S., Waterham, H. R., Keizer-Gunnink, I., Harder, W., and Veenhuis, G. A. (1996) *Appl. Microbiol. Biotechnol. 45*, 72−79.
37. Martemyanov, K. A., Spirin, A. S., and Gudkov, A. T. (1996) *Biotech. Lett. 18*, 1357−1362.
38. Darveau, R. P., Cunningham, M. D., Seachord, C. L., Cassiano-Clough, L., Cosand, W. L., Blake, J., and Watkins, C. S. (1991) *Antimicrob. Agents Chemother. 6*, 1153−1159.
39. White, S. H., Wimley, W. C., Ladokhin, A. S., and Hristova, K. (1998) *Methods Enzymol. 295*, 62−87.
40. Wolber, P. K., and Hudson, B. S. (1979) *Biophys. J. 28*, 197−210.
41. Schümann, M., Dathe, M., Wieprecht, T., Beyermann, M., and Bienert, M. (1997) *Biochemistry 36*, 4345−4351.
42. Förster, T. (1959) *Discuss. Faraday Soc. 27*, 7−17.
43. Cheung, H. C. (1991) in *Topics in Fluorescence Spectroscopy: Volume 2 Principles* (Lakowicz, J. R., Ed.) pp 127−176, Plenum Press, New York.

BI9811617